

submitted to NiM as part of special issue from International Conference on
Advanced Technology and Particle Physics held at Como, Italy in June, 1988.

The Central Tracking Detectors for DØ

A. Clark, F. Goozen, C. Klopfenstein, L.T. Kerth

S. Loken, M. Strovink, and T.G. Trippe

Lawrence Berkeley Laboratory

University of California, Berkeley, CA 94720 USA

J. Bantly, D. Buchholz, D. Claes, B. Gobbi, and S. Rajagopalan

Northwestern University

Evanston, IL 60208 USA

T. Behnke, O. Callot¹, J. Cochran, R. Engelmann, G. Finocchiaro,

D. Pizzuto, G. Rahal-Callot, M. Rijssenbeek, and F. Stocker

State University of New York at Stony Brook

Stony Brook, NY 11794-3800 USA

DISCLAIMER

This report was prepared as an account of work sponsored by an agency of the United States Government. Neither the United States Government nor any agency thereof, nor any of their employees, makes any warranty, express or implied, or assumes any legal liability or responsibility for the accuracy, completeness, or usefulness of any information, apparatus, product, or process disclosed, or represents that its use would not infringe privately owned rights. Reference herein to any specific commercial product, process, or service by trade name, trademark, manufacturer, or otherwise does not necessarily constitute or imply its endorsement, recommendation, or favoring by the United States Government or any agency thereof. The views and opinions of authors expressed herein do not necessarily state or reflect those of the United States Government or any agency thereof.

Abstract

Three types of drift chambers are being constructed for the Fermilab DØ experiment. The construction and readout of these chambers stress good spatial resolution, good two hit separation, and dE/dx . A 106 MHz FADC system with hardware zero suppression is being constructed to readout this system.

AC02-80ER10699

¹ also at Laboratoire de l'Accelérateur Lineaire, 91405 ORSAY France

MASTER

EP

1. Introduction

The $D\theta$ detector is presently being constructed to investigate $\bar{p}p$ interactions at Fermilab. Since this detector has no central magnetic field, the central tracking portion is very compact. It is designed for good spatial resolution of individual particles, good two track separation, and dE/dx to distinguish singly-ionizing tracks from doubly-ionizing tracks created by γ conversions. The details of the $D\theta$ detector are covered more completely elsewhere[1].

The central tracking detector consists of four distinct elements. Figure 1 shows a side view of one quarter of the central tracking detector. The vertex detector is a set of three layers of cylindrical drift chambers just outside of the beam tube. The transition radiation detector lies just outside of the vertex chamber and consists of three concentric layers of polypropylene foils followed by radial drift X-ray detectors. This detector is now completed and its test results are being covered in a separate presentation to this conference. Outside of the transition radiation detector is the outer central tracking detector. This cylindrical detector is comprised of four layers of axial wire chambers. In addition to these central detectors there are also the forward/backward drift chambers. These consist of two types of chambers, theta and phi. The theta chambers have wires aligned along cartesian coordinates and give a measure of a track's θ relative to the beam direction. The phi chambers have radial wires and measure the track's azimuthal angle ϕ . Each of the tracking detectors will be described in more detail.

2. Vertex Chambers

The vertex chambers, which are being constructed at Lawrence Berkeley Laboratory, have been tested at atmospheric pressure with dimethyl ether, a non-saturated gas[2]. The chambers are configured with jet chamber geometries with two planes of grid wires. Each basic cell has 8 sense wires, 18 field wires, and additional cathode and field cage wires. The cell geometry in the (r, ϕ) plane transverse to the beam direction is shown in figure 2. The sense wires are staggered by $\pm 100\mu\text{m}$ to resolve the left-right ambiguity. The wires are strung along the direction of the beam tube in three layers of basic cells. The maximum wire length is 110 cm. The three layers of basic cells are built between four carbon fiber cylinders. The parameters relevant to all three tracking chamber systems are listed in more detail in Table I.

3. Outer Central Chambers

The outer central drift chamber is under construction at Stony Brook, and three final modules have been tested extensively with cosmic rays. This chamber has four cylindrical layers, each one divided in 32 cells in the (r, ϕ) plane. Each cell contains 7 wires and 2 delay lines parallel to the beam direction. Each particle traversing this chamber will be seen by 28 sense wires. Embedded in the sidewalls of each cell are two delay lines for measurement of the longitudinal coordinate. Figure 3 shows a portion of the end plate with the outline for the sense wires, guard wires, and delay lines. The chamber operates at atmospheric pressure and has been tested with "Mark II" gas (3% CO₂, 4% CH₄, and 93% Ar) and P10 gas (90% Ar and 10% CH₄). The sense wires are staggered by $\pm 200 \mu\text{m}$ to resolve the left-right ambiguity and subsequent layers are shifted by a half cell. The basic cell is formed from rohacell covered with epoxy coated kevlar cloth and wrapped with a double layer of 0.002" Kapton. The field shaping electrodes are lines of conductive ink screen printed onto the Kapton and are linked internally to resistive dividers. Table I gives additional details about this detector. Results presented here for this chamber are mostly from the cosmic ray tests and are in good agreement with previous tests of prototype chambers at Brookhaven National Laboratory [3].

4. Forward Chambers

The forward drift chambers are actually of two types, one with a radial wire orientation and one with a wire orientation along cartesian coordinates, to measure principally the ϕ and θ angles, respectively. Figure 4 shows the wire orientation in both these types of chambers. Some earlier test results of a prototype chamber have already been published[3]. The phi chamber has 16 layers of radial sense wires of length 50 cm. The maximum drift distance is 5.3 cm. The chambers operate at atmospheric pressure with the same gas as the outer central drift chamber. The phi chamber is sandwiched between two theta chambers each with 8 layers of sense wires. Their orientation is shown in figure 4. The two theta chambers are rotated by 45° with respect to one another. The sense wires in both the phi and theta are staggered by $\pm 200 \mu\text{m}$. The full theta cells have two guard wires at ground potential between pairs of sense wires. The phi cell has a single guard wire between sense wires which is also held at ground potential. The top and bottom cell walls of the theta chambers are kevlar-coated rohacell which are covered with copper traces on Kapton to form the field-shaping electrodes. The side walls are 0.008" aluminum foil on Nomex honeycomb.

The cell walls on the phi are etched 0.001" aluminum strips on 0.005" G-10 to form the field-shaping electrodes. The tops and bottoms are kevlar coated Nomex honeycomb with copper traces on kapton. Table I also gives additional details about the forward chambers.

5. Electronics

The electronics for all the drift chambers are similar. The preamplifiers, which are based on the Fujitsu MB43458[4] quad common base amplifier in a surface mount package, are mounted in groups of eight channels on a hybrid that fits a regular 28-pin DIP socket together with input protection circuitry. This hybrid also has small coupling capacitors to inject test charges on each sense wire channel to verify the integrity of the whole electronics chain. The signals are carried via coaxial cables from the chambers over a distance of about 15 m to the shaping circuitry[5]. The shaping circuit contains a video amplifier, two pole-zero shaping circuits, a cable driving circuit, and circuitry to compensate for the coaxial cable attenuation. The gain and shaping components are mounted on a separate header printed circuit board for each channel so that they can be easily modified for each chamber to accommodate different gains and pulse shapes. The shaped signals are transported about 45 m to the digitizing circuitry on coaxial cables. The digitizers have 8 bit Sony flash analog to digital converters (FADC) operated at 106 MHz. To extend the effective range from 8 bits to 9.5 bits the FADC is preceded by a bilinear amplifying network with programmable gain [6]. To reduce the data collected to a manageable level the digitizer also contains a Fermilab designed zero suppression chip and memory to sparcify the data in real time as it is collected[7]. The zero suppression chip is programmable to the extent that its thresholds are set from memory to look for certain arrangements of the signal and the first difference of the signal to determine if the data should be retained for further analysis. An example of the digitizer output for the first eight wires in the phi forward chamber is shown in figure 5. The example shows the signal for a total of 5.2 μ s without the zero suppression being enabled. A second particle entered the chamber after the initial one and is visible late in the signal traces. Wire 0 also contains a delayed reference pulse which is used to set the initial time when the particle arrived at the chamber.

6. Spatial Resolution

The position resolution of these chambers has been measured under a variety of different conditions. The vertex chamber resolution was measured in a test beam at BNL.

with 8-bit 100Mhz FADC's. As with the other chambers the programs to find the hits in the data are based on looking at the successive first differences of the data to find where the leading edge of the pulses are located[8]. The accuracy of a single wire is obtained by examining the difference in time between any hit and the time average of the hits on the two neighboring wires. The final resolution has to be corrected since the rms of the residual includes contributions from all three wires and not just the one in question. For equally spaced wires this factor is just $\sqrt{2/3}$. Figure 6 shows this resolution after corrections versus the drift distance for the vertex chamber. A similar plot for the outer central drift chamber which was obtained with cosmic rays is shown in figure 7. Figure 8 shows the resolution for the forward drift chamber as obtained in a test beam at Fermilab. This resolution is worse than previously measured[3] due to electronic noise and is currently being investigated. The maximum drift distance for the outer central and forward chamber is 7 cm and 5.3 cm, respectively, while that of the vertex detector is 1.6 cm.

7. Two Particle Separation

The primary reason that we require FADCs as fast as 100 MHz is to be able to separate two closely spaced tracks in the data. As was shown earlier[3] this sampling frequency is not required for the position resolution, but rather for the two hit separation and the dE/dx . Figures 9 and 10 show the two hit separation limits for the vertex and forward drift chambers. These plots are obtained by superimposing tracks from one event onto another but at a known time from the first hits. This modified data is then processed again by the same hit finding routines to see how often they find the second hits as a function of the known time delay. The vertex chamber sees the second hit 84 ns (0.7 mm) later with a 90% efficiency. The outer central chamber and the forward chamber are quite similar with their wire spacing, gas gain and see the second hit 90% of the time after a 2 mm separation. These results were obtained without any pulse shaping and will improve with appropriate shaping.

8. dE/dx

The $D\theta$ detector does not have a central magnetic field. This means that e^+e^- pairs from γ conversions inside the central detector are most likely to overlap in space within the resolution of this detector (the transition radiation detector will allow us to identify the e^+ and e^-). If a γ converts in the outer wall of the TRD, the inner wall of the outer central

detector, or material in front of the forward chambers, the TRD is not effective to identify these electrons. The inner vertex detector will provide rejection of these tracks by the lack of a charged track. To provide additional rejection at large angle and in the forward direction where the vertex detector does not cover, it is necessary that the drift chambers be able to distinguish e^+e^- pairs from singly-ionizing particles. Figure 11 shows how well the outer central chamber identifies doubly ionizing tracks from singly-ionizing tracks. The data for this study was obtained by using a 0.8 GeV/c momentum proton beam and 6 GeV/c pion beam at BNL. The plot shows the average of the lowest 21 samples of the available 32 for the "electrons" (singly-ionizing pions) and "pairs" (doubly-ionizing low energy protons). If one requires to be able to identify singly-ionizing tracks with 95% efficiency, then less than 1% of the pairs will be misidentified as singly-ionizing tracks.

9. Alternate Coordinate Readout

Each of the drift chamber systems obtains one coordinate from the time of drift information. The wire stagger in each cell helps to resolve the left-right ambiguity inherent in the drift chambers. To obtain the second coordinate in the cells, along the direction of the wires, the vertex chamber relies on charge division and helical pad readouts. The sense wires are resistive so that by reading out and comparing the charge signal at each end of the wire the location of a hit can be calculated. The accuracy that is anticipated with this technique is ± 1 cm. This technique becomes confused when the cells occupancy exceeds several particles. To aid the charge division coordinate measurement, helical pads have been added to the vertex chamber. This technique has small rectangular pads that see an induced signal from a small portion of several sense wires. The pads are connected together in a helical pattern around the chamber. Each of the three layers in the vertex chamber has helical pads on the inner and outer wire of that layer except for the innermost layer which has none due to a lack of space. The pads are expected to locate the hits in the wires direction with an accuracy of ± 0.4 cm. The outer central chamber uses delay lines to resolve the location along the sense wire. Each of the four layers in this detector has a delay line embedded in the chamber wall located just below the inner wire and just above the outer wire. The delay lines accuracy has been measured to be better than ± 0.4 cm and is shown over a length of 1 m in figure 12. The forward theta chambers use the same delay lines. Each of the theta cells has one delay line located just underneath the last sense wire. The accuracy here will be the same as the outer central detector.

10. Summary

Each of the components of the central tracking chambers of the DØ experiment has been tested with particles. The position resolution in the vertex chamber is measured to be in the range of 30 to 80 μm over the drift distance of 2 to 11 mm. The outer central chamber has a measured accuracy of 170 to 190 μm over a drift distance up to 6.5 cm. The forward chambers have a similar position resolution. The delay lines give a resolution of approximately ± 0.4 cm along the directions of the sense wire. Construction is currently underway on all these chambers and it is anticipated that they will all be completed by the summer of 1989 in time for installation later that year.

Acknowledgements

This research was supported in part by the U. S. Department of Energy through Contract Nos. DE-AC03-76SF00098, DE-AC02-80ER10699, AND DE-AC02-76ER02289.

References

1. "The DØ Detector at the Fermilab Collider", Paul Grannis, Proceedings of Les Rencontres de Physique de la Vallée D'Aoste, May 1987 and "The DØ Design Report", Fermilab, November 1984 (unpublished).
2. A. R. Clark, F. Goozen, L. T. Kerth, C. Klopfenstein, S. C. Loken, M. Strovink, and T. G. Trippe, Nucl. Inst. and Meth., A261 (1987) 420.
3. D. Buchholz, D. Claes, B. Gobbi, S. Park, T. Behnke, M. Carcano, R. Engelmann, G. Finocchiaro, K. Nishikawa, and D. Pizzuto, Nucl. Inst. and Meth., A257, (1987) 556.
4. R. Yarema. IEEE Trans. Nucl. Sci. NS-33 (1986) 933.
5. "Central Tracking Detector Flash A/D Converter Buffer Circuit Summary", G. Saewert and B. Chase, internal DØ Note 669 (unpublished).
6. "Shaper Circuit Specification", D. Howard, internal DØ note (unpublished).

7. M.L. Martin, M.E. Johnson, M.J. Mayberry, and D.C. DeGroot, IEEE Trans. Nucl. Sci. NS-34 (1987) 258.
8. D. Schaile, O. Schaile, and J. Schwarz, Nucl. Inst. and Meth., A242, (1987) 247 and also references 2 and 3.

Table I
Detector Specifications

Vertex Chamber

Maximum length	116.8 cm
Radial Interval	3.7 to 16.2 cm
Number of cell layers	3
Maximum drift distance	16 mm
Radial wire interval	4.57 mm
Number of sense wires per cell	8
Number of sense wires	640
Number of helical pad readouts	768
Total number of readout channels	2048
Tested with gas	Dimethyl ether
Pressure of gas	atmospheric
Drift field	2.3 KV/cm
Sense wire potential	+2.5 KV
Diameter of sense wire	25 μ m NiCoTin
Diameter of guard wire	152 μ m Au-plated Al

Outer Central Drift Chamber

Length	179.4 cm
Radial interval	51.8 to 71.9 cm
Number of cell layers	4
Maximum drift distance	7 cm
Sense wire staggering	0.2 mm
Number of guard wires per sense wire	2
Radial wire interval	6 mm
Number of sense wires in cell	7
Number of sense wires	896
Number of delay lines	256
Total number of readout channels	1408
Tested with gas	P10 and Mark II
Pressure of gas	atmospheric
Drift field	650 V/cm
Sense wire potential	+1.5KV
Diameter of sense wire	0.03 mm

Diameter of guard wire 0.127 mm

Forward/ Backward Drift Chambers

Theta modules

z interval	104.8 to 111.2 and 128.8 to 135.2 cm
Radial interval	11 to 62 cm
Number of cells in radius	6
Maximum drift distance	5.3 cm
Sense wire staggering	0.2 mm
Number of guard wires per sense wire	2
Sense wire separation	8 mm
Number of sense wires in z per cell	8
Number of delay lines per cell	1
Number of sense wires per end	384
Number of delay line readout per end	96
Total number of readout channels per end	480
Tested with gases	P10 and Mark II
Pressure of gas	atmospheric
Drift field	1.0 KV/cm
Sense wire potential	+1.5KV
Diameter of sense wire	30 μ m
Diameter of guard wire	163 μ m

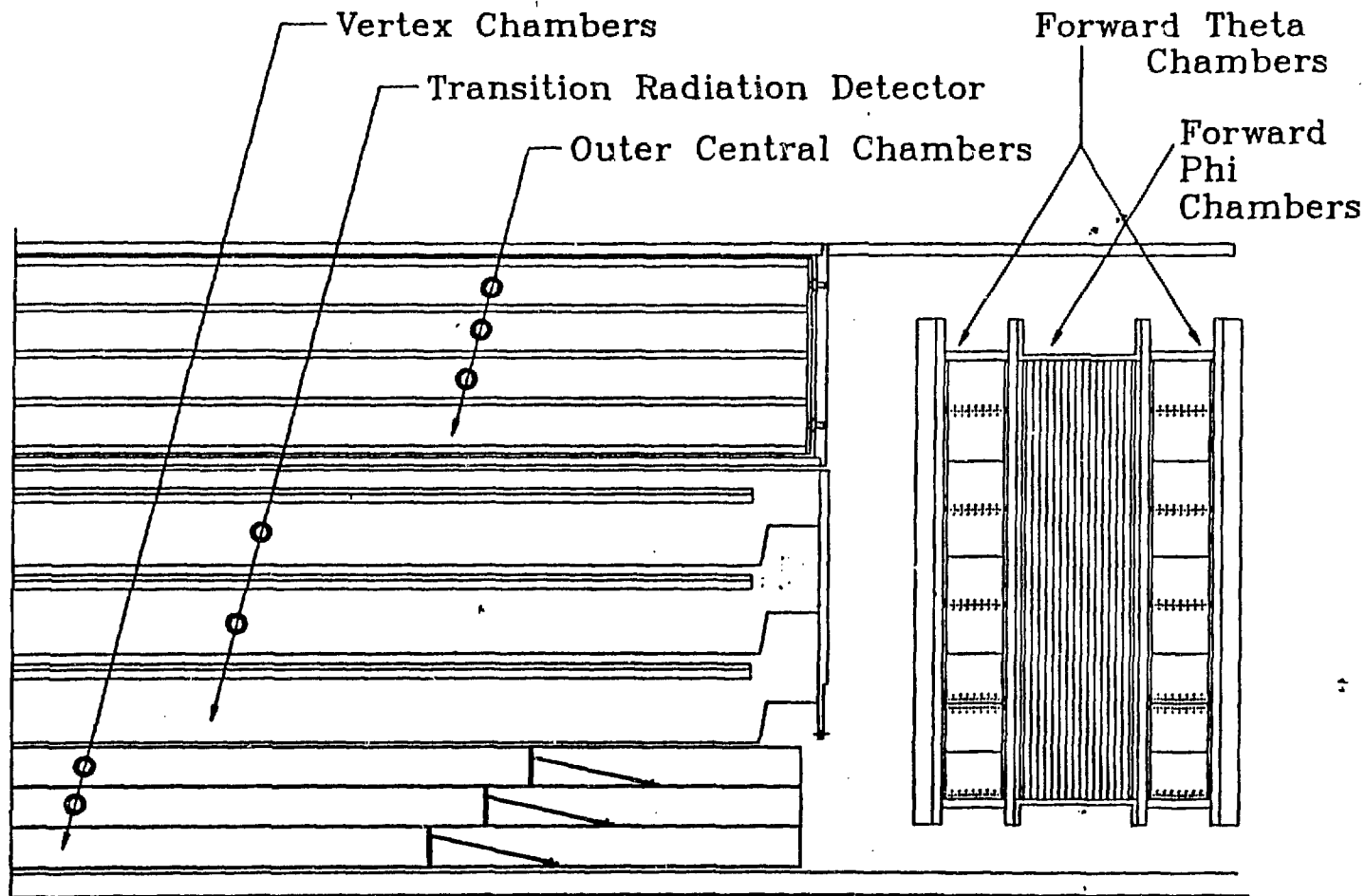
Phi Modules

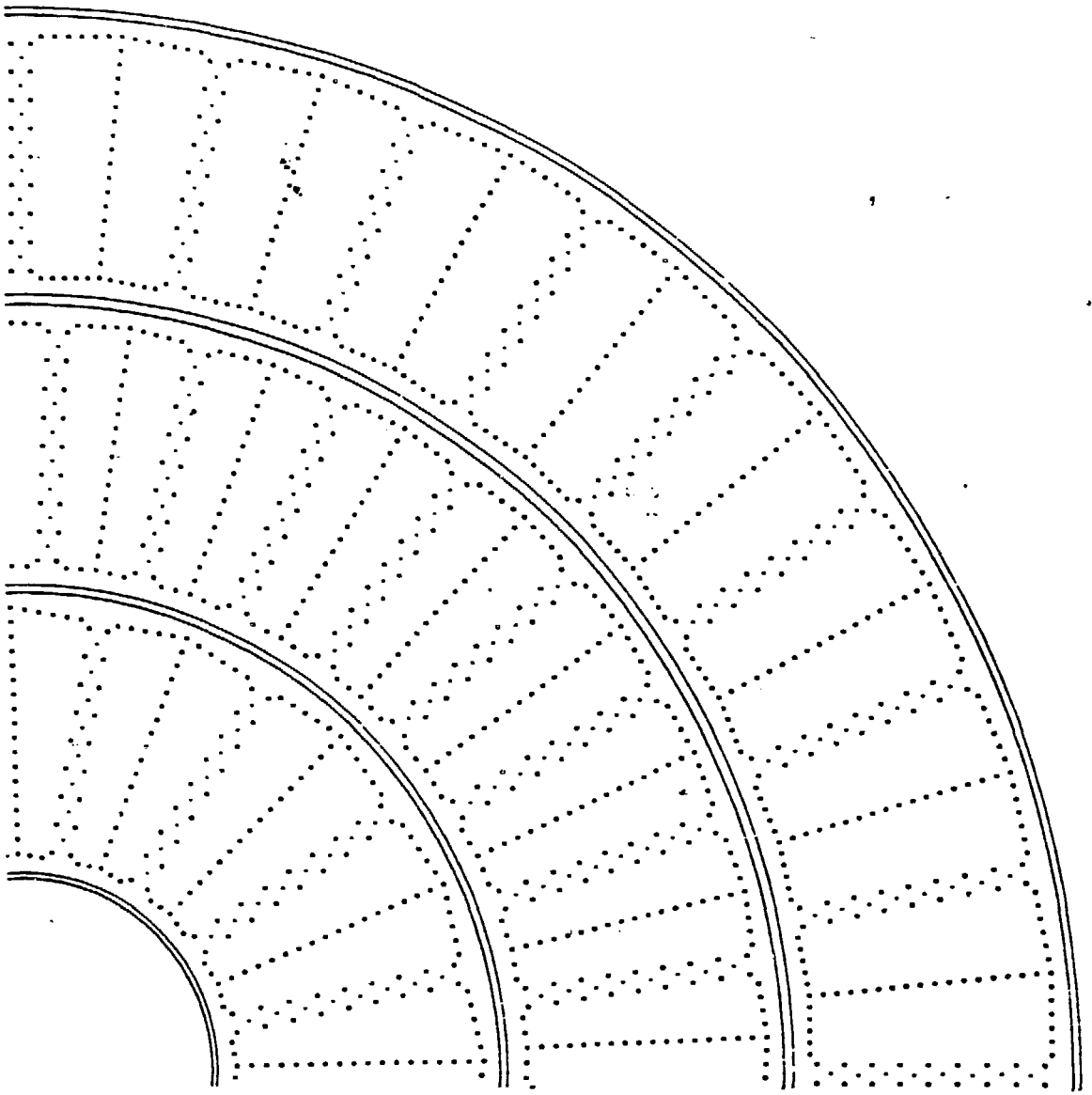
z interval	113.0 to 127.0 cm
Radial interval	11 to 61.3 cm
Maximum drift distance	5.3 cm
Sense wire staggering	0.2 mm
Number of guard wires per sense wire	1
Sense wire separation	8 mm
Number of wires in z per cell	16
Angular interval of cell	10°
Number of wires per end	576
Total number of readout channels per end	576
Tested with gas	Mark II

Pressure of gas	atmospheric
Drift field	1.0 KV/cm
Sense wire potential	+1.5KV
Diameter of sense wire	30 μ m
Diameter of guard wire	163 μ m

Figure captions

1. Side view of the central tracking portion of the DØ detector.
2. End view of one quarter of the wire plate for the vertex detector showing the three staggered layers.
3. View of the end of three segments of the four layers of the outer central tracking chamber showing the locations of sense and guard wires and delay lines.
4. View of the theta and phi chambers of the forward drift detector showing the beam view of the detectors. Some wires are indicated in this figure.
5. Example of the FADC output of 8 wires in the phi chambers. Two particles are visible within the 5.2 μ s visible in the plot. The sharp spike on channel 7 is a timing pulse superimposed on the data.
6. Single hit accuracy versus drift distance in the vertex detector.
7. Single hit accuracy versus drift distance in the outer central detector.
8. Single hit accuracy versus drift distance in the forward phi detector. The different symbols are for horizontal beam sweeps across different locations in the detector.
9. Efficiency for two particle identification versus the hit separation for the vertex detector.
10. Efficiency for two particle identification versus the hit separation for the forward theta detector.
11. dE/dx for simulated electrons and e^+e^- pairs as measured in the outer central detector.
12. Delay line resolution.





XBL 875-2345

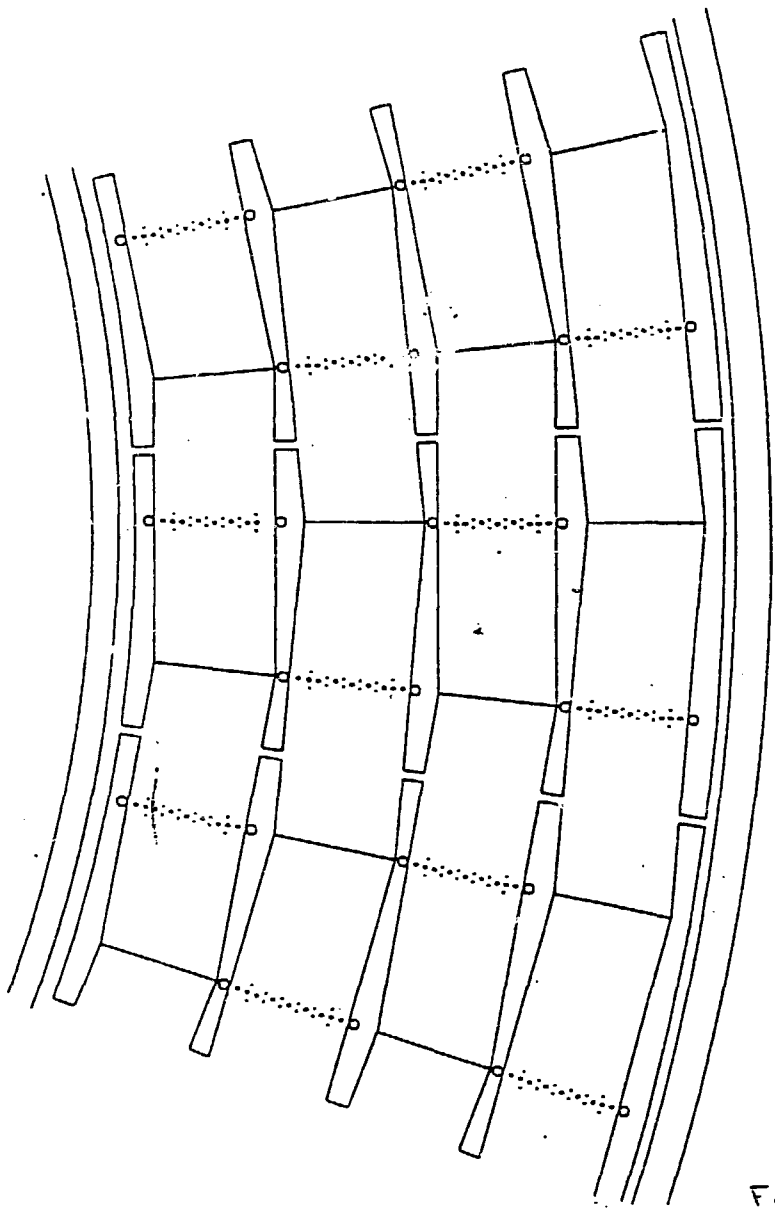
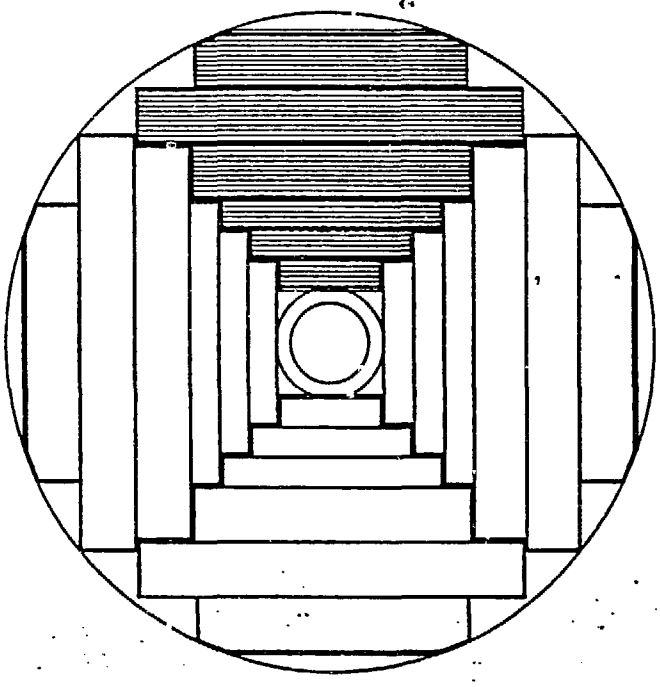
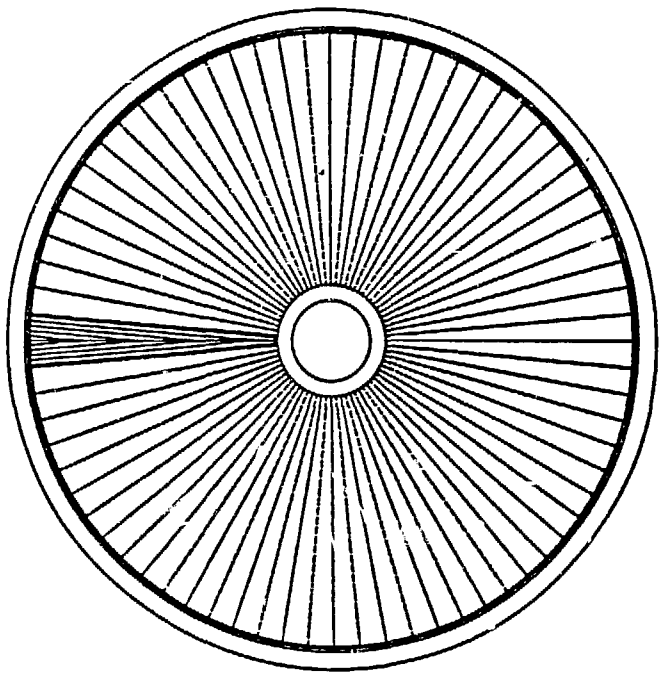


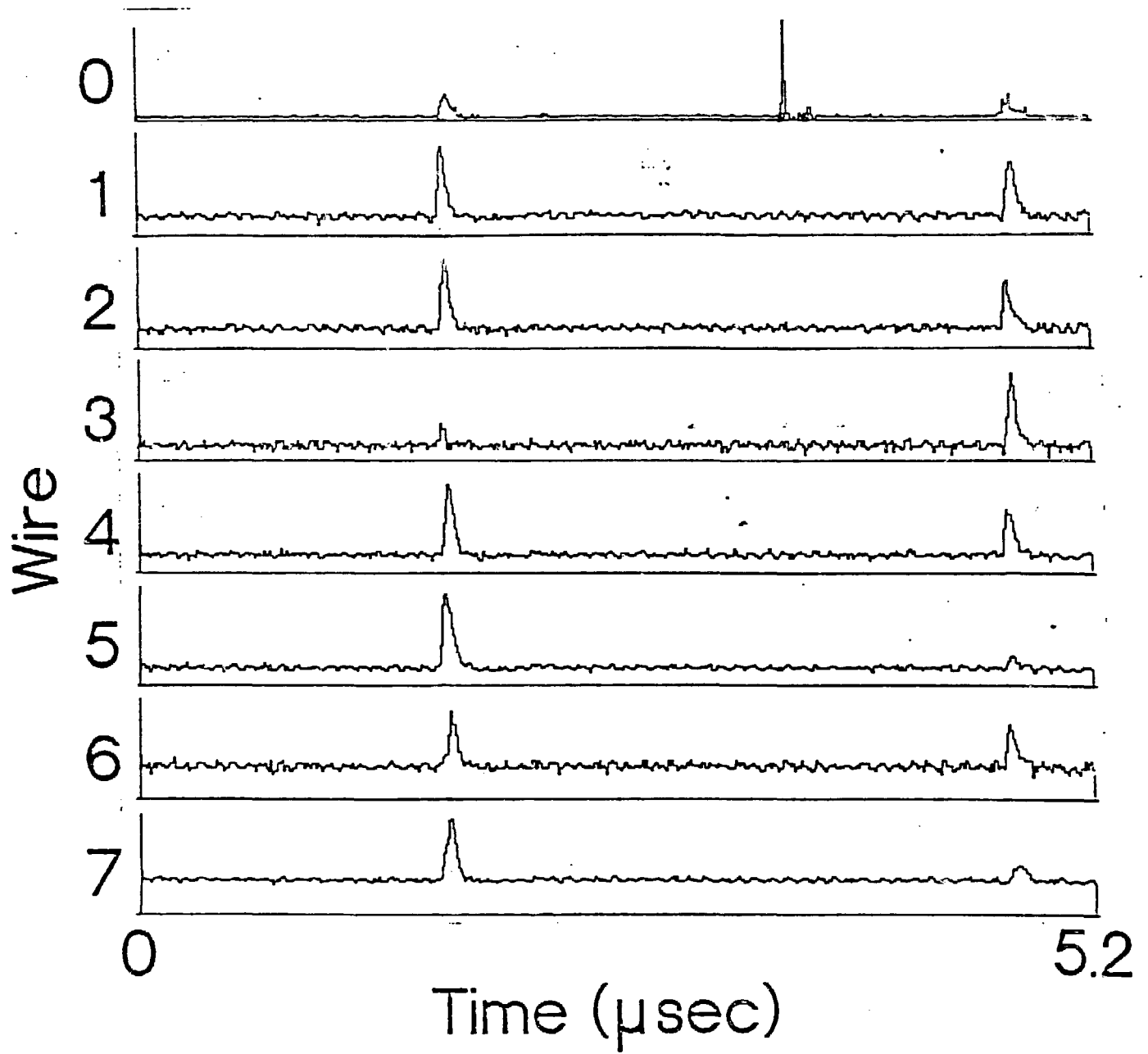
Figure 3

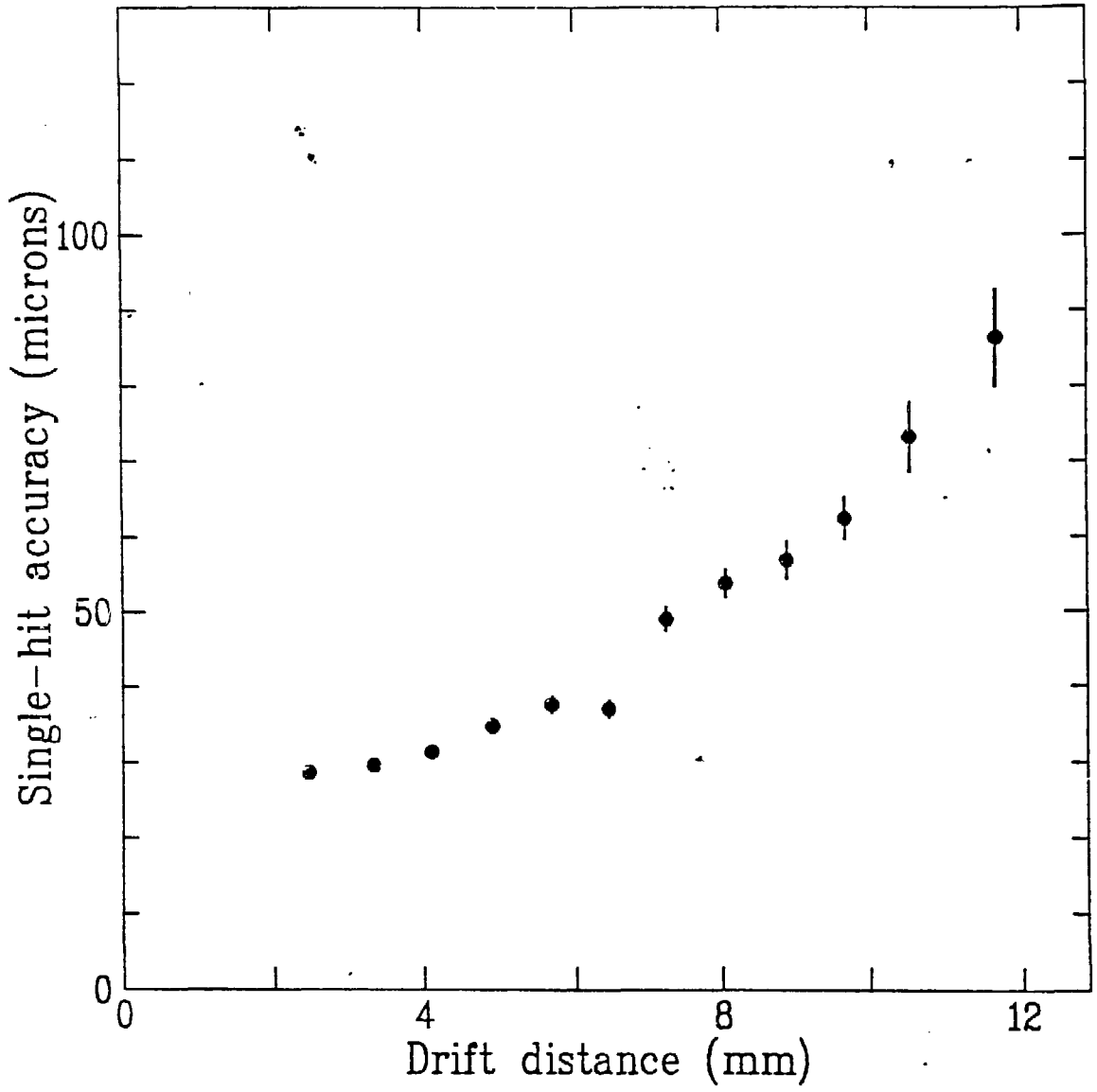
Theta



Phi







XBL 875-2344

DO CENTRAL DETECTOR

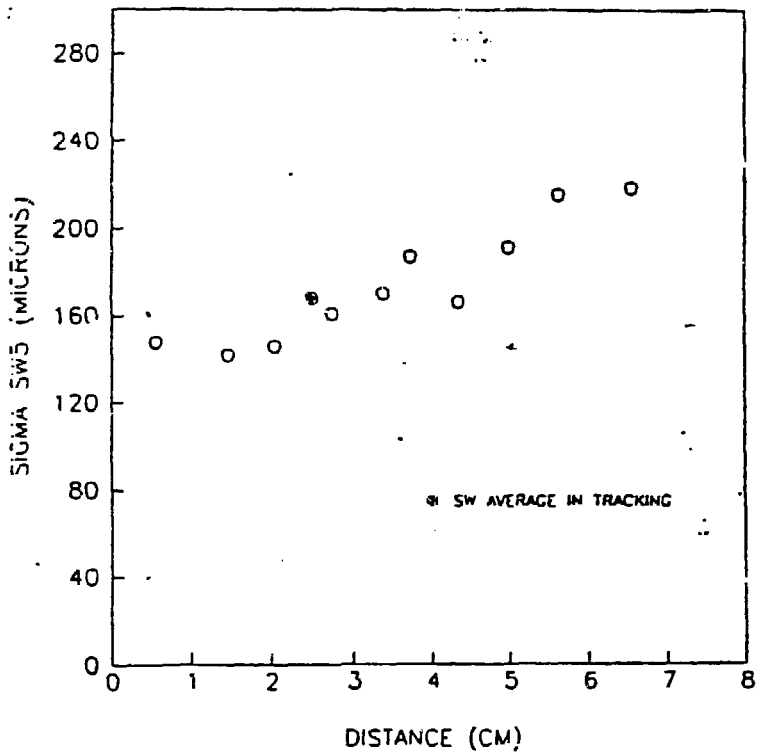
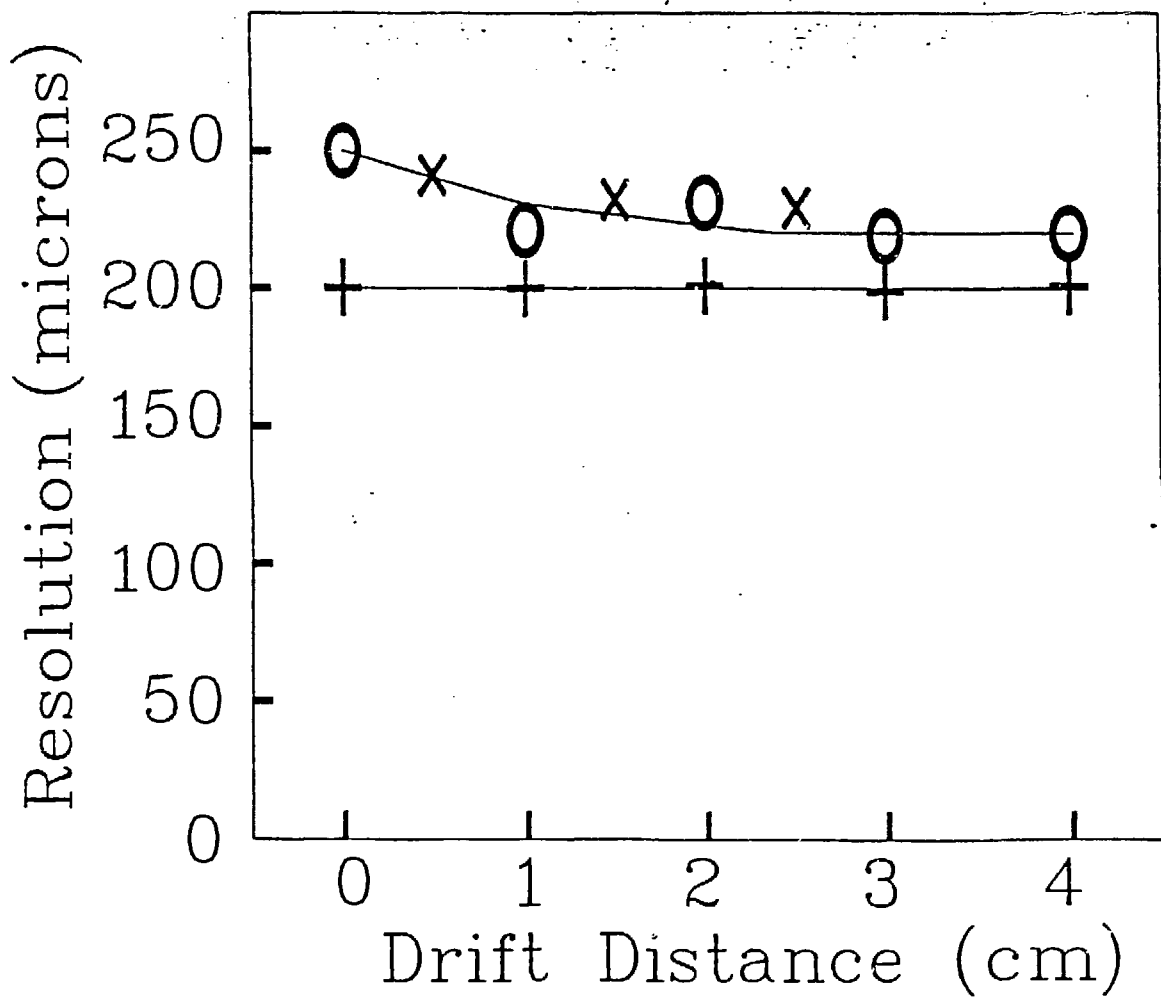
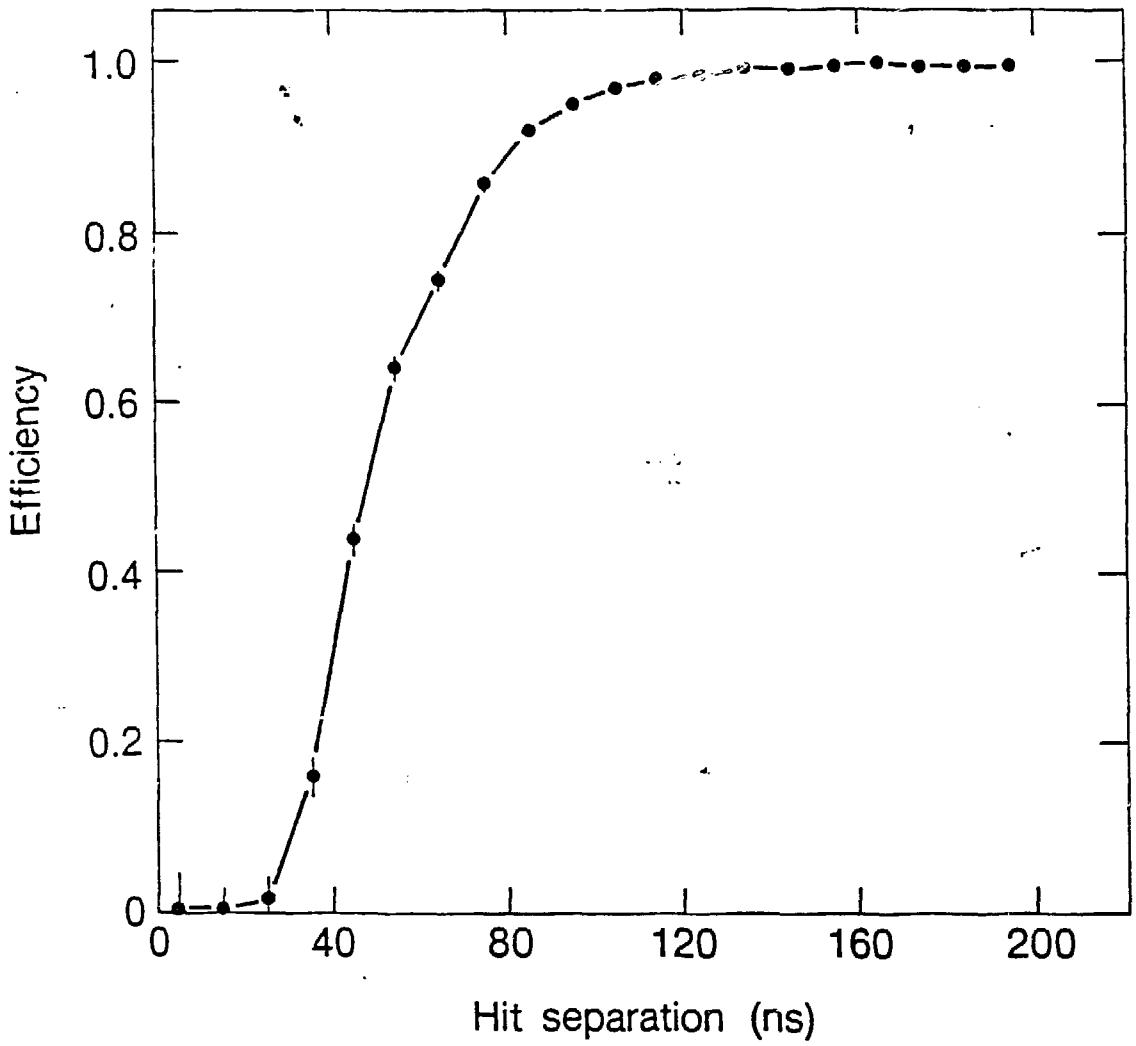
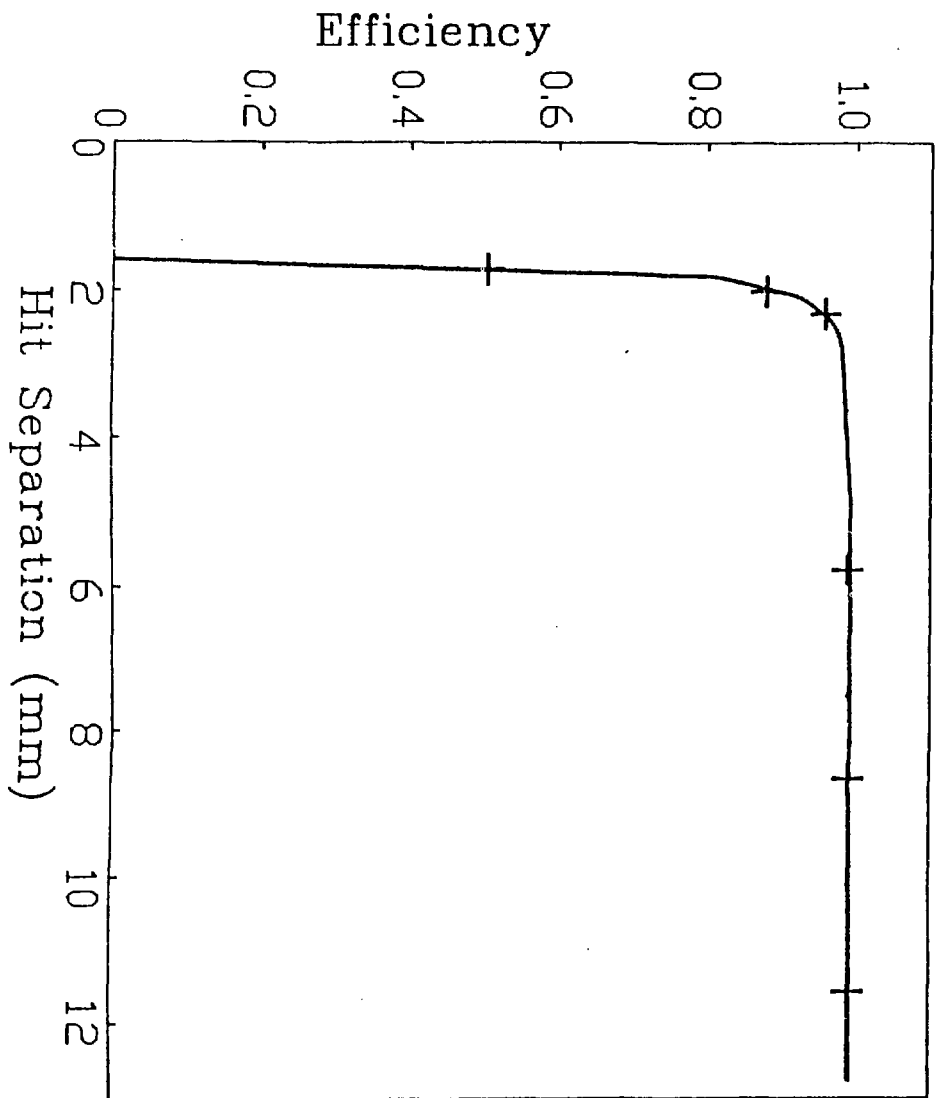


figure 7





XBL 875-9662



FROM BNL TEST

$4 \times 8 = 32$ samples (wires)

RUN 427 DO CENTRAL DETECTOR

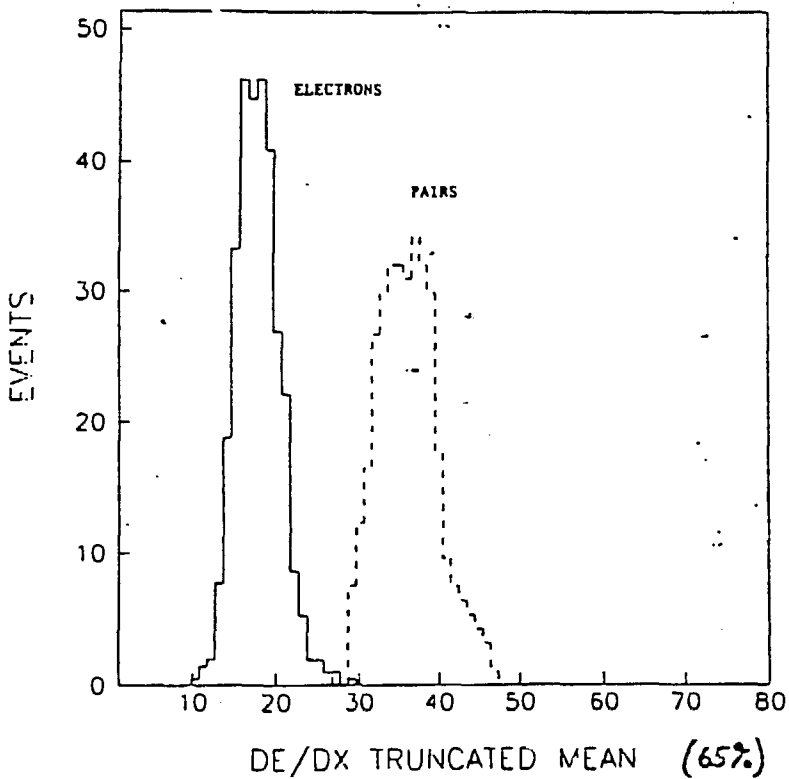
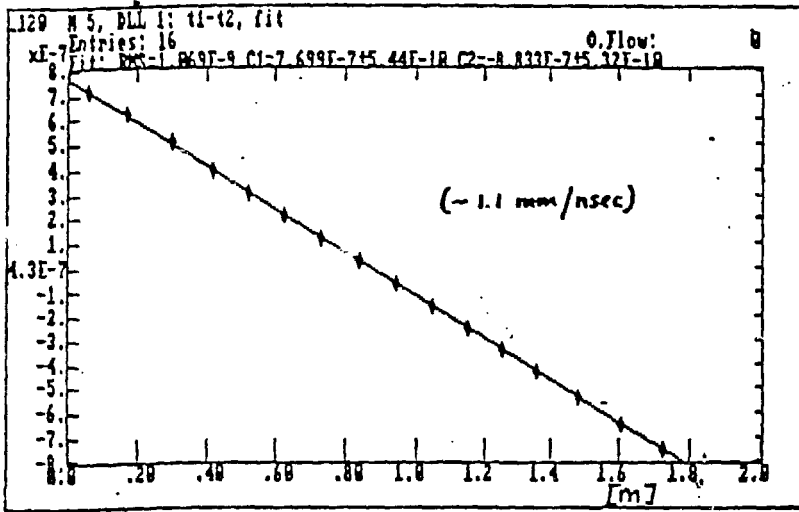


figure 11



[S]

[m]

Z